# Emergence and spread of feline infectious peritonitis due to a highly pathogenic canine/feline recombinant coronavirus

Charalampos Attipa[1,2,3◇*], Amanda S Warr[2◇*], Demetris Epaminondas[4], Marie O'Shea[2], Andrew J Hanton[2], Sarah Fletcher[2], Alexandra Malbon[13], Maria Lyraki[5], Rachael Hammond[1], Alexandros Hardas[6], Antria Zanti[3], Stavroula Loukaidou[3], Michaela Gentil[7], Danielle Gunn-Moore[1], Stella Mazeri[2], Christine Tait-Burkard[2*]

[1]Royal (Dick) School of Veterinary Studies, University of Edinburgh, Easter Bush, Midlothian, United Kingdom.

[2]The Roslin Institute, Royal (Dick) School of Veterinary Studies, University of Edinburgh, Easter Bush, Midlothian, United Kingdom.

[3]Vet Dia Gnosis Ltd, Limassol, Cyprus.

[4]Veterinary Services, Ministry of Agriculture, Natural Resources and Environment, Cyprus.

[5]Plakentia Veterinary Clinic, Athens, Greece.

[6]Department of Pathobiology and Population Sciences, Royal Veterinary College, Hatfield, Hertfordshire.

[7]Laboklin GmbH and Co KG, Bad Kissingen, Germany.

◇Contributed equally to this work. CA was responsible for epidemiology, pathology and sample/outbreak data collection. AW performed sequencing and data analysis thereof. Both are equally important, but the latter couldn't have happened without the first.

*Corresponding authors

Email: charalampos.attipa@ed.ac.uk (Epidemiology, pathology)

Email: Amanda.warr@roslin.ed.ac.uk (Sequencing, bioinformatics)

Email: christine.burkard@roslin.ed.ac.uk (General enquiries, sequence analysis, virology, structure)

## Abstract

Cross-species transmission of coronaviruses (CoVs) poses a serious threat to both animal and human health[1-3]. Whilst the large RNA genome of CoVs shows relatively low mutation rates, recombination within genera is frequently observed and demonstrated[4-7]. Companion animals are often overlooked in the transmission cycle of viral diseases; however, the close relationship of feline (FCoV) and canine CoV (CCoV) to human hCoV-229E[5,8], as well as their susceptibility to SARS-CoV-2[9] highlight their importance in potential transmission cycles. Whilst recombination between CCoV and FCoV of a large fragment spanning orf1b to M has been previously described[5,10], here we report the emergence of a novel, highly pathogenic FCoV-CCoV recombinant responsible for a rapidly spreading outbreak of feline infectious peritonitis (FIP), originating in Cyprus[11]. The minor recombinant region, spanning spike (S), shows 96.5% sequence identity to the pantropic canine coronavirus NA/09. Infection has rapidly spread, infecting cats of all ages. Development of FIP appears very frequent and sequence identities of samples from cats in different districts of the island is strongly supportive of direct transmission. A near cat-specific deletion in the domain 0 of S is present in >90% of FIP cats. It is unclear as yet whether this deletion is directly associated with disease development and may be linked to a biotype switch[12]. The domain 0 deletion and several amino acid changes in S, particularly the receptor binding domain, indicate potential changes to receptor binding and cell tropism.

## Main

Following two epidemics, SARS-CoV (2002-4) and MERS-CoV (2012-ongoing), and a pandemic of previously unseen proportions, SARS-CoV-2 (2019 onwards), coronaviruses no longer need lengthy introductions of importance and scale. They are not only present in the human population but also in wildlife[13-15], companion animals[16-19] and livestock[13,20,21], and in all species these viruses have major impacts. The innate ability of coronaviruses to recombine with other coronaviruses continues to fuel their species-switching ability. It is therefore not surprising that both human and animal coronaviruses are linked in complex transmission and evolution cycles[3,14,19,22].

FCoV is found across the globe. The virus exists in two biotypes with the main biotype, feline enteric coronavirus (FECV), showing low virulence, and clinical signs are typically limited to mild enteritis. The second biotype of FCoV, proposed to originate each time from a mutation in an FECV-infected cat (reviewed in [23]), is known as feline infectious peritonitis virus (FIPV). FIPV causes feline infectious peritonitis (FIP), which is a fatal disease if left untreated. Clinical signs include an abdomen swollen due to peritoneal fluid, fever, weight loss, lethargy, anorexia, dyspnea, ocular abnormalities and neurological signs[8,16,24,25]. Mutations in S or the accessory genes 3abc and 7ab of FCoV[8,16,23,26] are thought to result in changes to the virus's tropism from cells in the enteric tract to macrophages, resulting in the different disease presentation seen with

66 the two biotypes. This change in primary tropism also impacts the virus's ability to transmit from
67 cat to cat, with the main transmission pathway of FECV being fecal-oral and FIPV typically having
68 relatively poor transmission potential. Antivirals, including remdesivir and GS-441524 have
69 recently been successfully used to treat cats with FIP[27].

70 FCoV and CCoV both belong to the *Alphacoronavirus 1* species alongside the porcine transmissible
71 gastroenteritis virus (TGEV) and, probably, the never fully sequenced rabbit enteric
72 coronavirus[28,29]. Both FCoV and CCoV have evolved two different serotypes through complex
73 recombination events between the two viruses with a suspected gradual evolution from CCoV-II
74 to TGEV and the later S deletion to porcine respiratory coronavirus (PRCV)[23,30]. Whilst
75 recombination events between CCoV and FCoV have significantly contributed to the serotype
76 evolution and have been frequently described, so far, none of them led to enhanced
77 transmissibility of FIP beyond closest contact[10,23,31,32]. Similarly, recombination events have been
78 reported between CCoV and TGEV[33], the latter has been found to recombine with the
79 pedacoronavirus (alphacoronavirus genus) porcine epidemic diarrhea virus[6]. These observations
80 are particularly important in view of the *Alphacoronavirus 1*-related human infections recently
81 observed[19,22].

82 In 2023, we alerted the veterinary field to an outbreak of FIP in Cyprus, where there had been a
83 concerning increase in cases[11]. Cases were recorded as FIP only if they had compatible
84 clinicopathological signs and a positive RT-qPCR for FCoV in one of the following samples;
85 peritoneal fluid, pleural fluid, cerebrospinal fluid, fine needle aspiration biopsies, or tissue
86 biopsies from granulomatous lesions or positive FCoV immunohistochemistry (IHC) of
87 granulomatous lesions (IHC). RT-qPCR confirmed FIP cases had increased from three and four in
88 2021 and 2022, respectively, to 215 cases (186 thereof in 2023) from January 2023 to June 2024,
89 representing more than a 50-fold increase. The outbreak emerged in January 2023 in Nicosia, the
90 capital of Cyprus. By February the area of Nicosia recorded the peak number of cases in any
91 district (Figure 1A & B). The next highest number of cases was observed in Famagusta, which
92 peaked in March, and by then the outbreak had spread to all districts of the Republic of Cyprus.
93 (Supplementary Tables S1-6). In June and July there was a decline in RT-qPCR confirmed cases,
94 which coincided with a large media awareness campaign to alert veterinarians to the spread of
95 FIP[11]. This fall in cases was likely due to most veterinarians diagnosing cases based on
96 clinicopathological findings without performing PCR testing due to the additional financial cost.
97 On August 3rd, the Republic of Cyprus minister's cabinet approved the use of human coronavirus
98 medication stocks in cats with FIP. For veterinarians to have access to this medication, amongst
99 others, a PCR confirmation was required, reflecting the increased cases recorded during August
100 2023 (Figure 1A & B). The number of unreported cases in Cyprus remains very high, not least due

to the high number of feral cats. Estimates from the Pancyprian Veterinary Association indicate approximately 10,000 cases were presented in the veterinary clinics from January 2023 until July 2023 due to clinical signs of FIP. Furthermore, in October 2023, a first imported case of FIP was confirmed in the UK[34]. The most common clinical form of FIP was effusive (63.72%; Figure 1C), followed by neurological FIP (26.05%) and the non-effusive (dry) form (10.23%) (Supplementary table S3). Whilst the initial wave of infections appeared to slow down in August 2023, a second wave can be observed September 2023-March 2024 with the beginning of a third wave indicated from June 2024. The only distinctive feature of the second and third waves is a higher proportion of non-effusive forms (Supplementary tables S3-S5). Possible explanations for this include: an altered immune response from the host following initial seroconversion and re-infection;-that the non-effusive form takes longer to develop; or that cats presenting with the non-effusive form in the early stages of the outbreaks were not diagnosed due to their less common clinical signs.

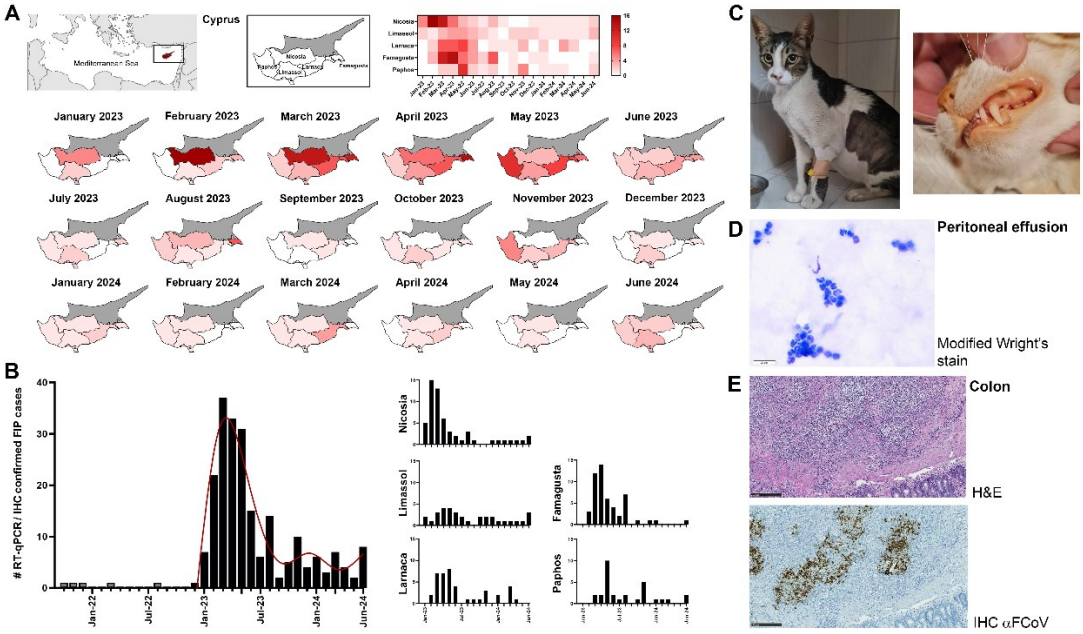


**Figure 1: Epidemiology and Pathology of the FIP outbreak in Cyprus, 2023-June 2024. A)** Distribution of RT-qPCR/IHCconfirmed FIP cases across Cyprus. First image locates Cyprus within the Eastern Mediterranean. Darker colors indicate higher numbers of confirmed cases over time within each district as highlighted in the overview heatmap with key. **B)** RT-qPCR/IHCconfirmed case rates resolved by time and province. A 6-knot spline interpolation highlights the three waves observed thus far. **C)** Clinical presentation of cats with FIP due to FCoV-23. Left; cat with the effusive form of FIP showing abdominal distention due to peritoneal effusion, an unkept coat, low body condition score, and poor muscle condition. Right; cat presenting with jaundice evidenced by yellow/orange discoloration of the mucous membranes and mucocutaneous junctions. Images courtesy of Dr Eva Georgiadi. **D)** Photomicrograph of fluid smear from a peritoneal effusion from a cat with confirmed FIP due to FCoV-23 infection. Non-degenerative neutrophils are present on a protein rich background shown using a Modified Wright's stain. Scale bar represents 20µm. E) Photomicrographs showing a section of colonic mucosa and submucosa from a cat with confirmed FIP due to FCoV-23 infection. Top; H&E-stained histology section shows coalescing infiltration of predominantly the submucosa by aggregates of primarily neutrophils and macrophages surrounded by fewer lymphocytes and plasma cells. The muscularis mucosae is disrupted by the inflammation. Bottom; Immunohistochemistry staining against FCoV in a histology section mirroring the above. Extensive positive FCoV cytoplasmic staining for cells at the center of each aggregate/pyogranuloma in cells with macrophage-like morphology. Scale bar represents 200µm.

129 Where peritoneal or pleural fluid was assessed by cytology, non-degenerative neutrophils
130 admixed with macrophages and small lymphocytes were seen in a protein rich background
131 (Figure 1D). 17 cases were assessed by histopathology, including intestinal mass (n=8), lymph
132 node (n=5), and kidney (n=4). All showed similar histological features, with multifocal to
133 coalescing, pyogranulomatous to necrotizing and lymphoplasmacytic inflammation (Figure 1E).
134 The angiocentric nature can be seen in some areas, whilst in others there is total effacement of
135 the tissue. Immunohistology for FCoV antigen demonstrated a heavy viral load within
136 intralesional macrophages (Figure 1E).

137 RNA samples were obtained from 163 confirmed FIP cases between 2021 and November 2023,
138 representing a mixture of geographic origin, sex, and clinical presentation (Supplementary Tables
139 S7-S12). There are inherent problems with obtaining sufficient read-depth with Illumina
140 sequencing on FIPV RNA samples. Therefore, we opted for cDNA/PCR-amplification-based
141 Nanopore sequencing to better understand the Cypriot outbreak and to determine if cat-to-cat
142 transmission is occurring. An initial crude approach based on alignments of reposited FCoV-1 and
143 FCoV-2 sequences yielded a mixed consensus sequence for the Cypriot outbreak strain, FCoV-23.
144 The consensus was used to design a new primer scheme for targeted amplification of FCoV-23 for
145 Oxford Nanopore-based sequencing. This yielded a total of 19 full-length genomes, 45 partial
146 sequences spanning a section of orf1b (~1,000 bp), 63 spanning the first part of S (~2,250 bp),
147 and 42 spanning ORFs 3c/E(4)/M(5) (~1,000 bp). These include samples from two cats
148 presenting with FIP following recent import from Cyprus to the UK. Other samples were degraded
149 or contained too few viral copies. None of the seven samples from before 2023 amplified
150 (Supplementary Tables S13-S18).

151 The partial S region sequence of the Cypriot/UK FCoV samples produced two distinct versions of
152 the S sequence. BLAST was used to identify close relatives of these S sequences. The first S
153 sequence is most closely related to an FCoV-1 (MT444152) with 79% similarity, which occurred
154 in one Cypriot and one UK-import sample. The others are almost entirely CCoV-2 S, flanked by
155 FCoV-1 sequence. The CCoV-2 sequence is most closely related to the NA/09 strain (JF682842), a
156 hypervirulent pantropic canine coronavirus (pCCoV)[35], at 96.5% sequence identity. As shown by
157 maximum likelihood analysis the S sequence is also closely related to other pCCoV S sequences
158 with only partial S sequences available (Figure 2, Supplementary Figure S1- S2). Interestingly, the
159 majority of samples contained a deletion at the N-terminus of S, which is analyzed in more detail
160 below. Except for the two samples highlighted above, all samples, including one UK-import case,
161 align most closely with a pCCoV S. This is likely a defining feature of the virus circulating in the
162 outbreak in Cyprus. In contrast, maximum likelihood trees of regions of ORF1b and ORF3c/E/M
163 (Figure 2, Supplementary Figures S3-S4) show clustering of all sequences with FCoV-1. Whilst

there appears to be more diversity in ORF1b, one must also consider the scale of the different trees.

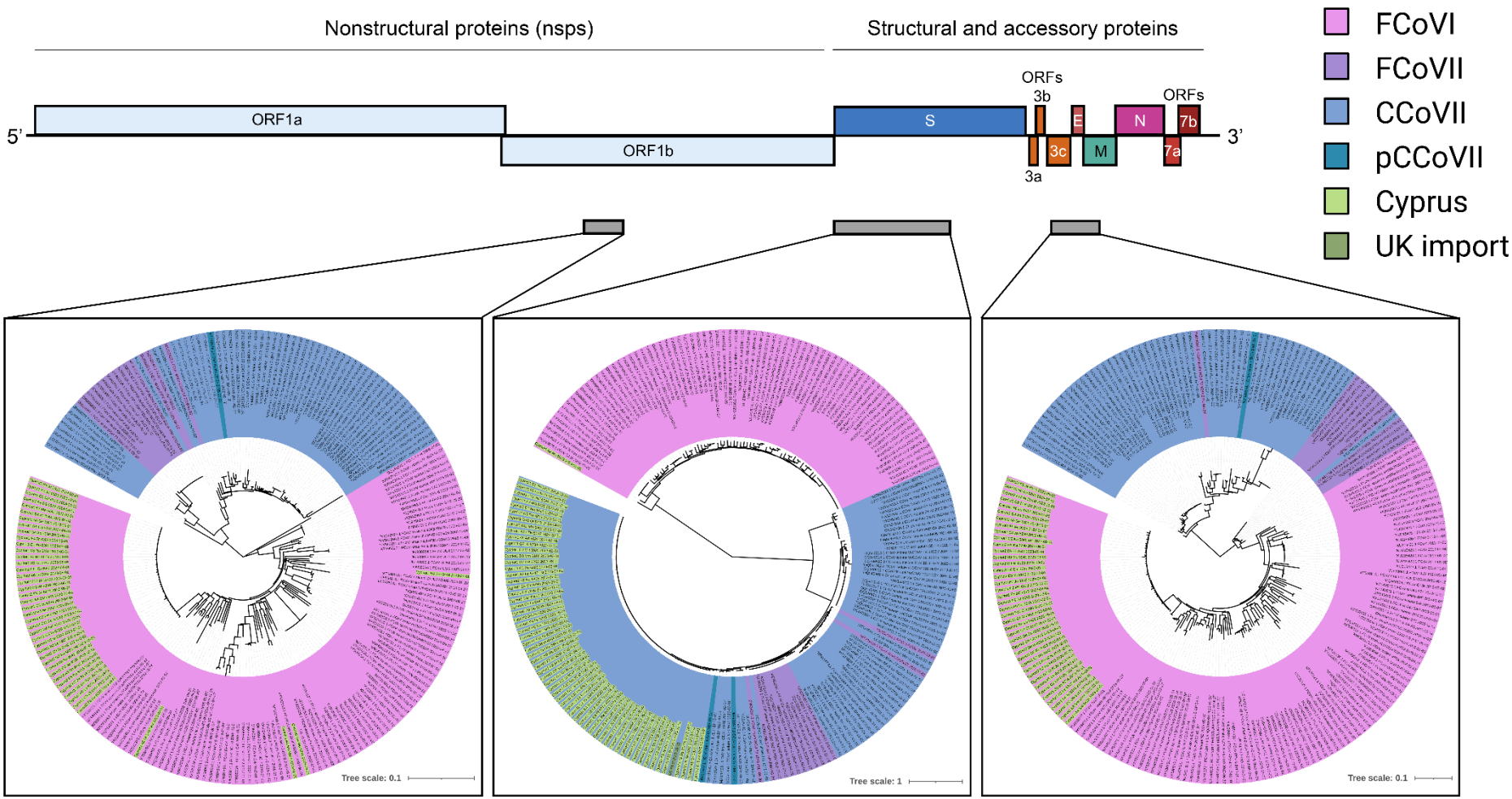


**Figure 2: Genomic sequence analysis of Cypriot/UK-import FCoV cases.** Sequences from three different genomic regions: Orf1b, S, and Orf3c/E/M, as indicated by the regions marked on the overview of the genome, were obtained through Nanopore sequencing from 45, 63, and 42, Cypriot and UK-import samples, respectively. Following initial BLAST analysis, maximum likelihood trees were generated including other FCoV and CCoV strains to assess genetic similarity of each region. CCoV-2 genomes are highlighted in blue with pCCoV-2 genomes within this region displayed in a darker blue. FCoV-1 genomes are highlighted in pink and FCoV-2 genomes in purple. Samples from Cyprus (green) and one UK-imported Cypriot cat (dark green) can be seen clustered with FCoV-1 sequences in the Orf1b and Orf3c/E/M regions. The S gene, however, clusters with CCoV-2, most closely with pCCoV-2. Different numbers of sequences are present in each tree due to missing sequence or poor sequence quality and/or alignments in genomes downloaded from NCBI, and due to not all regions being sequenced in all individuals from our samples.

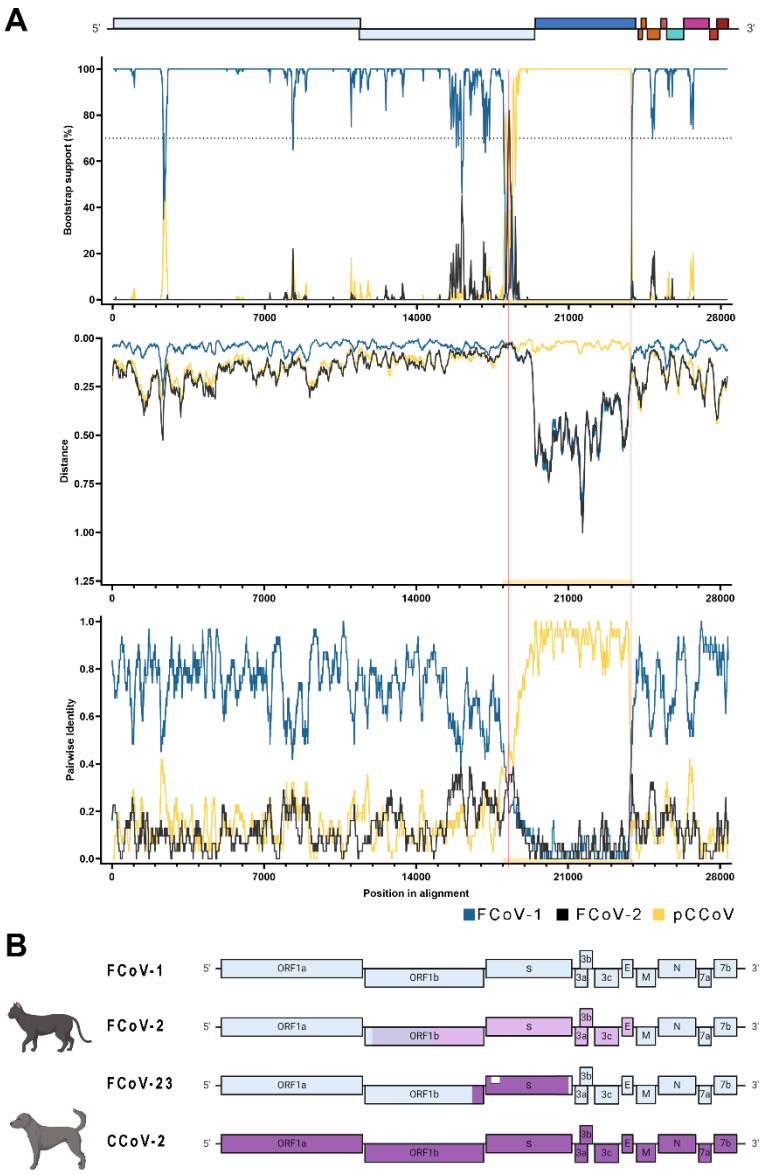


**Figure 3: Recombination analysis. A)** Visualizations of a recombination analysis carried out on the assembled FCoV-23 genome 2-C11 Re 10276 and representative genomes of FCoV-1 (blue), FCoV-2 (black) and pCCoV (yellow). The yellow panel shows the likely recombination break region, with a red vertical line showing the likely break point. The first panel shows the results of the Bootscan analysis, the second panel shows the sequence distance, and the third panel shows the RDP pairwise identity analysis. All three panels show good support for the recombination between FCoV-1 and pCCoV. These results are further supported by high statistical likelihood of recombination shown in Supplementary Table S21. Also see Supplementary Figures S6&7 and Table S21 for recombination analysis of a representative domain 0-deletion FCoV-23. **B)** Schematic representation of major recombinations observed in FCoV and CCoV. A common ancestral origin virus is thought to have given rise to the original FCoV-1 and CCoV-1 types with further evolution in CCoVs yielding CCoV-2 and CCoV-1/2 serotypes. FCoVs are thought to have recombined with CCoV-2 to form FCoV-2. FCoV-2/CCoV-2 recombinations have shown to have different recombination points as highlighted by the different colorations (reviewed in [23]). The Cypriot FCoV strain, termed FCoV-23, is a recombinant between an FCoV-1 strain and a S recombination with a pantropic CCoV-2, pCCoV. Furthermore, deletion variants are observed in a majority of sequenced cases (white box and Figure 4).

186 A recombination analysis was carried out comparing the FCoV-23 genome using representative
187 full-length sequence 2-C11 Re 10276 with FCoV-1, FCoV-2 and CCoV-2 strain CB/05, since NA/09
188 is not available as a complete genome. Figure 3A visualizes the Bootscan[36] analysis, the RDP5[37]
189 analysis and the pairwise distances between the sequences. Significant p-values supporting the
190 recombination were reported by multiple methods as listed in Supplementary Table S19. The
191 MaxChi[38] breakpoint matrix is available in Supplementary Figure S6. The recombination is very
192 clear and includes a small region of the ORF1b gene and the majority of S with breakpoints around
193 location 18,420 and 23,880. Figure 3B shows the historical break points between FCoV-1 and
194 CCoV-2 that created FCoV-2 alongside the recombination identified in FCoV-23.

195 Supplementary Figure S5 furthermore shows a neighbor joining tree for FCoV-23 along with
196 other members of *Alphacoronavirus 1* and a distantly related Canine Respiratory Coronavirus as
197 an outgroup. The assembled genome clusters with representatives of FCoV-1, similar to the
198 clustering of the amplicons outside of S.

199 The main determinant in disease development and transmission of FCoV-23 appears to be the S
200 recombination. One of the main suggested determinants of biotype changes, the furin cleavage
201 site (FCS) at the S1/S2 interface[23,26] is absent in FCoV-2 and also FCoV-23. An interesting
202 observation, however, is that the majority of samples (>90%) show a deletion in domain 0 (ΔD0),
203 strongly resembling the deletion observed in TGEV and PRCV (Figure 4A). Interestingly, whilst
204 the rest of the genome of FCoV-23 is highly conserved, the domain 0 deletion appears to be almost
205 cat-specific (Figure 4B). This indicates that this mutation occurs in host rather than being
206 transmitted. However, the only two fecal samples (also affected by sampling bias; <6% of our
207 samples are feces-derived) where sequences could be obtained show ΔD0. An in-host mutation
208 further begs the question of whether ΔD0 is associated with disease development. Unfortunately,
209 all our samples so far are from symptomatic, confirmed FIPV cases and further investigation is
210 required to answer this question.

211 In other coronaviruses, including TGEV[39] and CCoV-HuPn-2018[40], domain 0 was shown to bind
212 sialosides. Modelling the structure of S against the closely related, experimentally confirmed
213 CCoV-HuPn-2018 S[40] shows a much more compact conformation for ΔD0 S and similarity to a
214 structural prediction based on a "swung-out" or a "proximal" confirmation template (Figure 4C,
215 Supplementary Figure S8). A number of amino acid changes were observed between "classical"
216 FECV-2 and FIPV-2 S. In particular domains A, B, and the receptor binding domain (RBD) show a
217 number of class-changing amino acid changes distinct from FCoV-2 S (Figure 4A). Modelling the
218 RBD changes against the structure highlights changes at positions 546 and 595, as well as 556,
219 603, and 636 as being potentially strongly influential to receptor binding properties (Figure 4D).

Previously indicated key proteins for biotype switch S, Orf3abc and 7b were compared to the recently published computational analysis of mutations observed in FECV versus FIPV by Zehr *et al.*[26]. The suggested key determinant of FIPV in the FCoV-2 S, position 1404, shows a new amino acid, leucine instead of valine, in FCoV-23. However, this section of spike is derived from FCoV-1. It is therefore unclear how this recombination may impact overall functionality in the context of the rest of S being FCoV-2-like. Other positions in S show a mixture of FIPV versus FECV tendencies (Supplementary Table S23). Whilst a new mutation was identified in Orf3a and b, no specific indications of pathogenesis could be determined (Supplementary Table S24). Similarly, in Orf7b, two new mutations but no indication of pathogenesis could be identified (Supplementary Table S25).

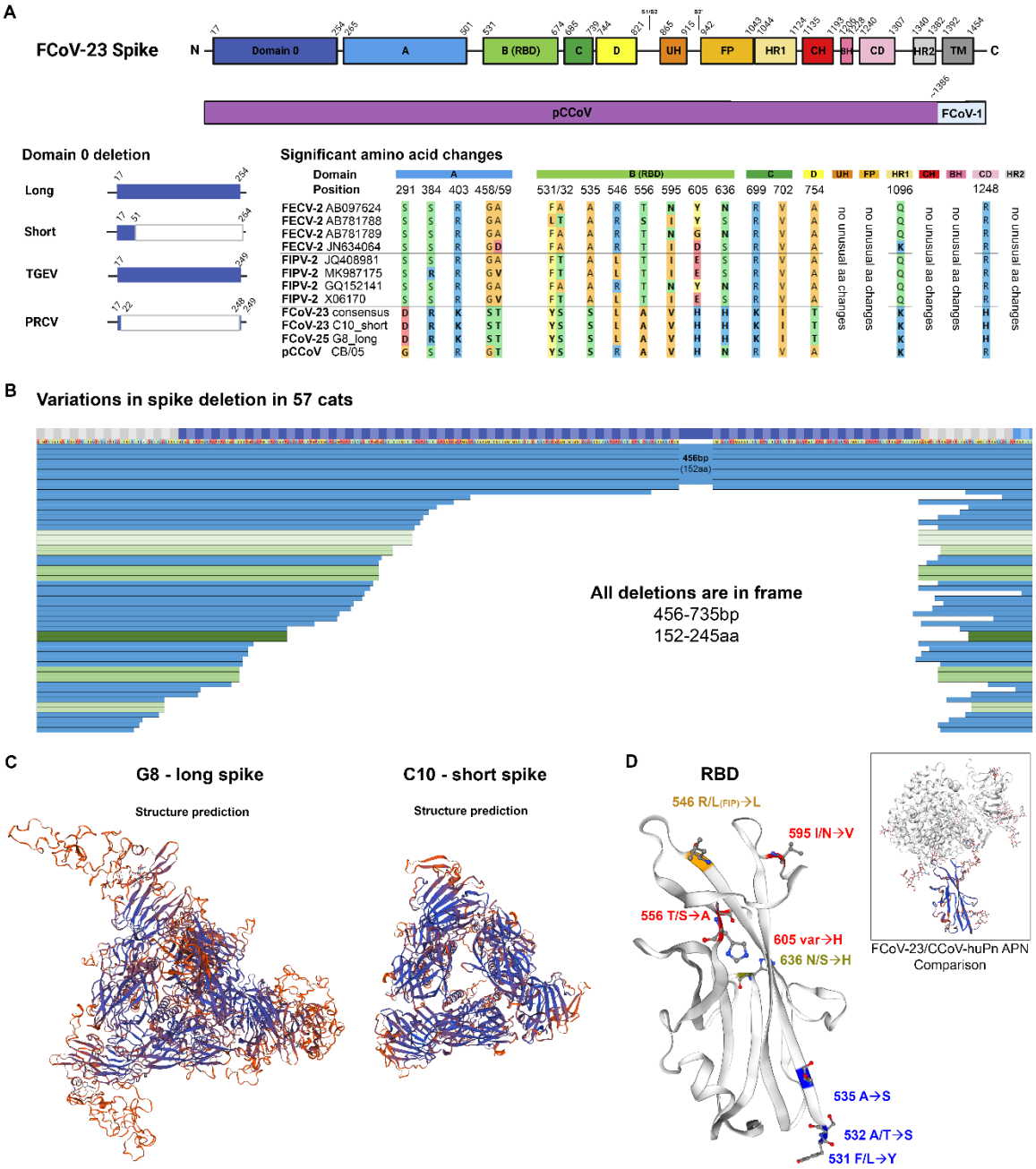

**Figure 4: Protein sequence and structural analysis of FCoV-23 Spike. A)** Analysis of the different domains of FCoV-23 S. Domain 0 in its full-length version shows high similarity to CB/05 pCCoV; however most prominent is the large, variable deletion between aa11-265 strongly resembling the deletion previously observed between the TGEV and PRCV S. Multi-sequence alignment was performed against four confirmed FECV-2 and four confirmed FIPV-2 mirroring sequences used for computational analysis by Zehr *et al.*[26]. Highlighted are amino acid changes with significant change against FCoV-2s and also position 546, where a Leucin is more predominant in FIPV rather than FECV sequences. Colors are following the RasMol amino acid color scheme. **B)** Domain 0 S deletions from 57 cats (8 full length) are shown from the beginning of S to amino acid 267. Sequences are ordered by the shortest 3'/N-terminal sequence. Identical deletions are highlighted in shades of green. All deletions show a multiplicity of 3 resulting in in-frame deletions. **C)** Structural modelling of the "full-length" or long S version, represented by sample G8, and the "domain 0 deletion" or short version, represented by sample C10. Samples were modelled against the CCoV-HuPN-2018, experimentally determined S in the swung out confirmation 7usa.1.A[40]. The proximal confirmation and comparisons may be found in Supplementary Figure 8. Colors indicate confidence with blue highlighting strong and red highlighting weak confidence. **D)** Modelling or amino acid changes on a structural prediction of the FCoV-23 RBD against CCoV-HuPN-2018 7u8I.1.B. Significant amino acid changes as identified in A) are highlighted with side-chains in blue for variations to FCoVIIs distant from the RBD, red for variations close to the RBD, orange for the variation at aa546 similar to FIPV-2, and olive for the variation differing both from FCoVII and pCCoV. A comparison showing a confidence model of the FCoV-23 RBD structure prediction paired with the CCoV-HuPN-2018-canine aminopeptidase N (APN) is shown for orientation and binding visualization in the top right corner. Colors indicate confidence with blue highlighting strong and red highlighting weak confidence.

## Discussion

Recombination within the *Alphacoronavirus 1* species has been frequently observed previously and has even given rise to the FCoV-2 serotype[5,23,24](Figure 3B) in cats. Even complex recombination between FCoV-1 and CCoV has previously been observed[10]. However, in this work, we have identified a new subtype of FCoV that has recombined with a hypervirulent strain of pCCoV. The recombinant, which we propose naming FCoV-23, shows clearly distinct properties from previously observed FCoV infections. The sequence similarity found between FCoV-23 and CCoVII is higher than would be expected without an additional, recent recombination event.

Our data suggest that there is direct transmission of FCoV-23 between cats based on high sequence identity (>99.17% genome-scale including varying S-deletion length, Supplementary figures S9 & S10), high viral loads (RT-qPCR only) in feces, as well as the wave-like movement of disease across the island. However, it is unclear whether this virus still needs a biotype change to result in FIP. A potential reason for differences in pathogenicity may be the acquiring of a deletion of S domain 0. This is observed in >90% of FIP cases studied here and in a near host-specific pattern. More work is needed to assess the properties of ΔD0 S, as well as investigation into asymptomatic carriers. Whilst alphacoronaviruses show great cross-neutralizing activity[40], the onset of FIP appears rapid and shows little discrimination in age of the infected cats highlighting that FCoV-23 is able to circumnavigate preexisting immunity. If a biotype change is required, it clearly happens far more frequently in FCoV-23 than any of the previously observed FCoV infections. We therefore must study FCoV-23 to gain further understanding of the FECV/FIPV change. The scale of this FIP outbreak has not been observed previously. Concerningly, Cyprus has a high population of unowned cats that are frequently relocated to other parts of Europe, and

271 the wider world. The risk of spreading this outbreak is significant as evidenced by the first
272 confirmed UK case[34].

273 CCoV infections in dogs are typically self-limiting, producing mild enteritis or presenting
274 asymptomatically. Previous work on the FCoV-23 close relative strain, CCoV NA/09 and CB/05,
275 found that the virus was hypervirulent and infected a range of organs in canine hosts. CCoV
276 typically infects cells of the enteric tract, but pCCoVs were shown to spread to a range of internal
277 organs, including intestine, lung, spleen, liver, kidney, lymph nodes, brain, and even T and B cells
278 [35,41-43]. CB/05 has also been identified as responsible for small outbreaks[41].

279 The clinical signs of FCoV-23 are similar to those observed in classical FIP cases. However, FIP
280 infection itself already shows a strong pantropism, affecting many organs in infected cats[25]. What
281 is remarkable is the high number of FCoV-23 positive cells observed in immunohistochemistry
282 samples (Figure 1C). This is indicative of high viral loads, but must be validated through
283 quantification. Furthermore, a relatively high percent (Supplementary Table 4) of confirmed
284 cases in Cyprus was presented with neurological signs (26%), which is almost double of what
285 would be expected with classical FIP (14%)[27]. This may be due to increased awareness of
286 presentation or be inherent to FCoV-23 neurotropism; however, further investigation is required.

287 Significant changes to the S protein in FCoV-23 may provide some clues as to the enhanced
288 pathogenicity of this virus. FCoV-23, like other FCoV-2s and CCoV-2, does not contain an FCS at
289 the S1/S2, and the related virus CCoV-HuPn-2018 was experimentally found to be uncleaved[40].
290 Uncleaved S has been shown to be more stable than cleaved and could enhance fecal shedding
291 and stability in the environment[44]. Conversely, the cleavage at S1/S2 may facilitate the movement
292 of the N-terminal domains and allow the RBD to adopt the receptor-binding-competent form.
293 However, the deletion of domain 0 may compensate for the increased rigidity. Whilst a similar
294 deletion between TGEV and PRCV was initially indicated as the determinant between a primarily
295 enteric and primarily respiratory tropism, respectively[45,46], a recent study shows a different result
296 *in vivo*[47]. Sialoside binding is an important feature of coronavirus infections and may contribute
297 to intracellular spread[48]. It is then all the more surprising that FCoV-23 loses the sialoside-binding
298 domain 0. However, whilst binding to sialosides can enhance virus attachment and entry into host
299 cells, binding to sugars can lead to increased retention of virus on producer cells. Whilst some
300 viruses, like influenza, solve this issue by encoding their own sugar-cleaving enzyme,
301 neuraminidase, coronaviruses must find a balance through modifying glycoprotein binding[49].
302 Losing domain 0 could therefore be a trade-off to enhance virus release. This may be
303 compensated by the earlier discussed enhanced flexibility of S and increased binding efficiency
304 at the RBD through mutation. These are manifold in the FCoV-23 pCCoV recombinant and in

305 particular mutations at position 546 (already possibly associated with FIP) and 595 are likely to
306 have a strong impact on aminopeptidase N receptor binding (Figure 4C).

307 Recombination between FCoV-1 and pCCoVs is not surprising in that i) such recombinations have
308 been observed before, and ii) pCCoVs have evolved in Greece and south eastern Europe[35,42].
309 However, the emergence of pCCoV in Greece happened over 1 years ago so the question as to why
310 this happened now is unclear. One possible explanation is the "right mutation, right time, right
311 place" theory. Recombination between feline and canine coronaviruses happen frequently but as
312 previous reports show, they rarely spread. Introduction of a more successful, spreading variant
313 to a dense population, like the cats in Cyprus, may be sufficient to allow this virus to cause an
314 outbreak. However, the acquisition of a likely in-host deletion adds a further level of concern to
315 coronavirus evolution. These viruses already show a mutation rate, similar to influenza viruses
316 (despite proofreading)[50], high prevalence for recombination[51], and here we could show that they
317 are able to acquire significant in-host INDELs that may completely change their cell binding
318 properties and tropism.

319 This paper reports the emergence of a new *alphacoronavirus 1* feline/canine coronavirus that
320 shows high spreading potential with the associated pathology of lethal FIP if left untreated.
321 Further investigations into the properties of this new virus are now essential. Whilst antivirals,
322 including GS-441524 and molnupiravir were successfully used to treat many cats affected by
323 FCoV-23, early treatment is essential but associated costs can be prohibitive. Prevention of spread
324 and the development of new vaccines are important to stop this epizootic virus from spreading
325 beyond Cyprus.

## Acknowledgements

The authors like to thank the Pancyprian Veterinary Association and all the veterinarians in Cyprus for sample submission. We would like to thank Dr Sam Lycett, The Roslin Institute, The University of Edinburgh for advice on sequence analysis.

## Author contributions

Conceptualization, C.A., A.W., D.G-M., S. M. and C.T-B.; Methodology, C.A., A.W., S.M., and C.T-B. ; Validation, C.A., A.W., S.M. and C.T-B.; Formal Analysis, A.W., S.M. and C.T-B.; Investigation, C.A., A.W., D.E., A.H., M.O., S.F. , A.M., M.L., R.H., C.T-B.; Resources, C.A., A.W., D.E., M.L., A.H., A.Z., S.L., M.G. and C.T-B.; Data Curation, A.W., S.M., and C. T-B.; Writing – Original Draft Preparation, C.A., A.W., and C.T.B.; Writing – Review & Editing, C.A., A.W., S.F., D.G-M., S.M. and C.T-B.; Visualization, A.W., S.M. and C.T-B.; Supervision, C.A. and C.T-B.; Project Administration, C.A. and C.T-B.; Funding Acquisition, C.A., and C.T-B.

## Funding

This work was supported by EveryCat Health Foundation award number EC23-OC1 (C.A., D.G-M., C.T-B.), Vet Dia Gnosis Ltd (C.A.). This research was funded by the BBSRC Institute Strategic Programme grant funding to the Roslin Institute, grant numbers BBS/E/D/20241866, BBS/E/D/20002172, and BBS/E/D/20002174 (C.T-B.).

## Competing interests

Laboklin GmbH & Co. KG is a veterinary laboratory offering diagnostic services, including bacteriological and molecular biological examinations. Vet Dia Gnosis LTD is offering veterinary pathology diagnostic services only. The co-author M.G. is employed by Laboklin GmbH & Co. KG. The co-authors C.A. and S.L. are the co-founders of Vet Dia Gnosis LTD. C.A. is an external collaborator of Vet Dia Gnosis LTD whilst S.L. and A.Z. are employed by Vet Dia Gnosis LTD.

352 **References**


353 1 Olival, K. J. *et al.* Host and viral traits predict zoonotic spillover from mammals. *Nature* **546**,
354 646-650 (2017). https://doi.org:10.1038/nature22975
355 2 Zhou, P. *et al.* Fatal swine acute diarrhoea syndrome caused by an HKU2-related coronavirus
356 of bat origin. *Nature* **556**, 255-258 (2018). https://doi.org:10.1038/s41586-018-0010-9
357 3 Nova, N. Cross-Species Transmission of Coronaviruses in Humans and Domestic Mammals,
358 What Are the Ecological Mechanisms Driving Transmission, Spillover, and Disease Emergence?
359 *Front Public Health* **9**, 717941 (2021). https://doi.org:10.3389/fpubh.2021.717941
360 4 Muller, N. F., Kistler, K. E. & Bedford, T. A Bayesian approach to infer recombination patterns
361 in coronaviruses. *Nat Commun* **13**, 4186 (2022). https://doi.org:10.1038/s41467-022-31749-
362 8
363 5 Herrewegh, A. A., Smeenk, I., Horzinek, M. C., Rottier, P. J. & de Groot, R. J. Feline coronavirus
364 type II strains 79-1683 and 79-1146 originate from a double recombination between feline
365 coronavirus type I and canine coronavirus. *Journal of virology* **72**, 4508-4514 (1998).
366 https://doi.org:10.1128/JVI.72.5.4508-4514.1998
367 6 Boniotti, M. B. *et al.* Porcine Epidemic Diarrhea Virus and Discovery of a Recombinant Swine
368 Enteric Coronavirus, Italy. *Emerging infectious diseases* **22**, 83-87 (2016).
369 https://doi.org:10.3201/eid2201.150544
370 7 Pedersen, N. C., Ward, J. & Mengeling, W. L. Antigenic relationship of the feline infectious
371 peritonitis virus to coronaviruses of other species. *Archives of virology* **58**, 45-53 (1978).
372 https://doi.org:10.1007/BF01315534
373 8 Pedersen, N. C. A review of feline infectious peritonitis virus infection: 1963-2008. *Journal of*
374 *feline medicine and surgery* **11**, 225-258 (2009). https://doi.org:10.1016/j.jfms.2008.09.008
375 9 Kannekens-Jager, M. M. *et al.* SARS-CoV-2 infection in dogs and cats is associated with contact
376 to COVID-19-positive household members. *Transbound Emerg Dis* **69**, 4034-4040 (2022).
377 https://doi.org:10.1111/tbed.14713
378 10 Terada, Y. *et al.* Emergence of pathogenic coronaviruses in cats by homologous recombination
379 between feline and canine coronaviruses. *PLoS One* **9**, e106534 (2014).
380 https://doi.org:10.1371/journal.pone.0106534
381 11 Attipa, C. *et al.* Concerning feline infectious peritonitis outbreak in Cyprus. *Vet Rec* **192**, 449-
382 450 (2023). https://doi.org:10.1002/vetr.3143
383 12 Jaimes, J. A. & Whittaker, G. R. Feline coronavirus: Insights into viral pathogenesis based on
384 the spike protein structure and function. *Virology* **517**, 108-121 (2018).
385 https://doi.org:10.1016/j.virol.2017.12.027
386 13 Amer, H. M. Bovine-like coronaviruses in domestic and wild ruminants. *Anim Health Res Rev*
387 **19**, 113-124 (2018). https://doi.org:10.1017/S1466252318000117
388 14 Woo, P. C., Lau, S. K., Huang, Y. & Yuen, K. Y. Coronavirus diversity, phylogeny and interspecies
389 jumping. *Exp Biol Med (Maywood)* **234**, 1117-1127 (2009). https://doi.org:10.3181/0903-MR-
390 94
391 15 Small, J. D. & Woods, R. D. Relatedness of rabbit coronavirus to other coronaviruses. *Adv Exp*
392 *Med Biol* **218**, 521-527 (1987). https://doi.org:10.1007/978-1-4684-1280-2_68
393 16 Gao, Y. Y. *et al.* An updated review of feline coronavirus: mind the two biotypes. *Virus Res* **326**,
394 199059 (2023). https://doi.org:10.1016/j.virusres.2023.199059
395 17 Haake, C., Cook, S., Pusterla, N. & Murphy, B. Coronavirus Infections in Companion Animals:
396 Virology, Epidemiology, Clinical and Pathologic Features. *Viruses* **12** (2020).
397 https://doi.org:10.3390/v12091023
398 18 Pedersen, N. C. An update on feline infectious peritonitis: virology and immunopathogenesis.
399 *Vet J* **201**, 123-132 (2014). https://doi.org:10.1016/j.tvjl.2014.04.017
400 19 Vlasova, A. N. *et al.* Animal alphacoronaviruses found in human patients with acute respiratory
401 illness in different countries. *Emerg Microbes Infect* **11**, 699-702 (2022).
402 https://doi.org:10.1080/22221751.2022.2040341

20 Saif, L. J. Animal coronaviruses: what can they teach us about the severe acute respiratory syndrome? *Rev Sci Tech* **23**, 643-660 (2004). https://doi.org:10.20506/rst.23.2.1513

21 Wang, Q., Vlasova, A. N., Kenney, S. P. & Saif, L. J. Emerging and re-emerging coronaviruses in pigs. *Curr Opin Virol* **34**, 39-49 (2019). https://doi.org:10.1016/j.coviro.2018.12.001

22 Corman, V. M., Muth, D., Niemeyer, D. & Drosten, C. Hosts and Sources of Endemic Human Coronaviruses. *Adv Virus Res* **100**, 163-188 (2018). https://doi.org:10.1016/bs.aivir.2018.01.001

23 Jaimes, J. A., Millet, J. K., Stout, A. E., Andre, N. M. & Whittaker, G. R. A Tale of Two Viruses: The Distinct Spike Glycoproteins of Feline Coronaviruses. *Viruses* **12** (2020). https://doi.org:10.3390/v12010083

24 Le Poder, S. Feline and canine coronaviruses: common genetic and pathobiological features. *Advances in virology* **2011**, 609465 (2011). https://doi.org:10.1155/2011/609465

25 Tasker, S. *et al.* Feline Infectious Peritonitis: European Advisory Board on Cat Diseases Guidelines. *Viruses* **15** (2023). https://doi.org:10.3390/v15091847

26 Zehr, J. D. *et al.* Natural selection differences detected in key protein domains between non-pathogenic and pathogenic feline coronavirus phenotypes. *Virus Evol* **9**, vead019 (2023). https://doi.org:10.1093/ve/vead019

27 Taylor, S. S. *et al.* Retrospective study and outcome of 307 cats with feline infectious peritonitis treated with legally sourced veterinary compounded preparations of remdesivir and GS-441524 (2020-2022). *Journal of feline medicine and surgery* **25**, 1098612X231194460 (2023). https://doi.org:10.1177/1098612X231194460

28 Descoteaux, J. P. *et al.* An enteric coronavirus of the rabbit: detection by immunoelectron microscopy and identification of structural polypeptides. *Archives of virology* **84**, 241-250 (1985). https://doi.org:10.1007/BF01378976

29 Lefkowitz, E. J. *et al.* Virus taxonomy: the database of the International Committee on Taxonomy of Viruses (ICTV). *Nucleic Acids Res* **46**, D708-D717 (2018). https://doi.org:10.1093/nar/gkx932

30 Whittaker, G. R., Andre, N. M. & Millet, J. K. Improving Virus Taxonomy by Recontextualizing Sequence-Based Classification with Biologically Relevant Data: the Case of the Alphacoronavirus 1 Species. *mSphere* **3** (2018). https://doi.org:10.1128/mSphereDirect.00463-17

31 Wang, Y. T., Su, B. L., Hsieh, L. E. & Chueh, L. L. An outbreak of feline infectious peritonitis in a Taiwanese shelter: epidemiologic and molecular evidence for horizontal transmission of a novel type II feline coronavirus. *Vet Res* **44**, 57 (2013). https://doi.org:10.1186/1297-9716-44-57

32 Chang, H. W., de Groot, R. J., Egberink, H. F. & Rottier, P. J. Feline infectious peritonitis: insights into feline coronavirus pathobiogenesis and epidemiology based on genetic analysis of the viral 3c gene. *J Gen Virol* **91**, 415-420 (2010). https://doi.org:10.1099/vir.0.016485-0

33 Decaro, N. *et al.* Recombinant canine coronaviruses related to transmissible gastroenteritis virus of Swine are circulating in dogs. *Journal of virology* **83**, 1532-1537 (2009). https://doi.org:10.1128/JVI.01937-08

34 Maggi, R. G. *et al.* Vector-borne and other pathogens of potential relevance disseminated by relocated cats. *Parasit Vectors* **15**, 415 (2022). https://doi.org:10.1186/s13071-022-05553-8

35 Ntafis, V. *et al.* Molecular characterization of a canine coronavirus NA/09 strain detected in a dog's organs. *Archives of virology* **157**, 171-175 (2012). https://doi.org:10.1007/s00705-011-1141-6

36 Martin, D. P., Posada, D., Crandall, K. A. & Williamson, C. A modified bootscan algorithm for automated identification of recombinant sequences and recombination breakpoints. *AIDS Res Hum Retroviruses* **21**, 98-102 (2005). https://doi.org:10.1089/aid.2005.21.98

452 37 Martin, D. P. *et al.* RDP5: a computer program for analyzing recombination in, and removing
453 signals of recombination from, nucleotide sequence datasets. *Virus Evolution* **7** (2020).
454 https://doi.org:10.1093/ve/veaa087
455 38 Smith, J. M. Analyzing the mosaic structure of genes. *J Mol Evol* **34**, 126-129 (1992).
456 https://doi.org:10.1007/bf00182389
457 39 Schultze, B. *et al.* Transmissible gastroenteritis coronavirus, but not the related porcine
458 respiratory coronavirus, has a sialic acid (N-glycolylneuraminic acid) binding activity. *Journal*
459 *of virology* **70**, 5634-5637 (1996). https://doi.org:10.1128/JVI.70.8.5634-5637.1996
460 40 Tortorici, M. A. *et al.* Structure, receptor recognition, and antigenicity of the human
461 coronavirus CCoV-HuPn-2018 spike glycoprotein. *Cell* **185**, 2279-2291 e2217 (2022).
462 https://doi.org:10.1016/j.cell.2022.05.019
463 41 Buonavoglia, C. *et al.* Canine coronavirus highly pathogenic for dogs. *Emerging infectious*
464 *diseases* **12**, 492-494 (2006). https://doi.org:10.3201/eid1203.050839
465 42 Decaro, N. *et al.* Molecular characterisation of the virulent canine coronavirus CB/05 strain.
466 *Virus Res* **125**, 54-60 (2007). https://doi.org:10.1016/j.virusres.2006.12.006
467 43 Marinaro, M. *et al.* Prolonged depletion of circulating CD4+ T lymphocytes and acute
468 monocytosis after pantropic canine coronavirus infection in dogs. *Virus Res* **152**, 73-78 (2010).
469 https://doi.org:10.1016/j.virusres.2010.06.006
470 44 Wrobel, A. G. *et al.* SARS-CoV-2 and bat RaTG13 spike glycoprotein structures inform on virus
471 evolution and furin-cleavage effects. *Nat Struct Mol Biol* **27**, 763-767 (2020).
472 https://doi.org:10.1038/s41594-020-0468-7
473 45 Sanchez, C. M. *et al.* Targeted recombination demonstrates that the spike gene of
474 transmissible gastroenteritis coronavirus is a determinant of its enteric tropism and virulence.
475 *Journal of virology* **73**, 7607-7618 (1999). https://doi.org:10.1128/JVI.73.9.7607-7618.1999
476 46 Sanchez, C. M., Pascual-Iglesias, A., Sola, I., Zuniga, S. & Enjuanes, L. Minimum Determinants
477 of Transmissible Gastroenteritis Virus Enteric Tropism Are Located in the N-Terminus of Spike
478 Protein. *Pathogens* **9** (2019). https://doi.org:10.3390/pathogens9010002
479 47 Wang, G. *et al.* The N-Terminal Domain of Spike Protein Is Not the Enteric Tropism
480 Determinant for Transmissible Gastroenteritis Virus in Piglets. *Viruses* **11** (2019).
481 https://doi.org:10.3390/v11040313
482 48 Qing, E., Hantak, M., Perlman, S. & Gallagher, T. Distinct Roles for Sialoside and Protein
483 Receptors in Coronavirus Infection. *mBio* **11** (2020). https://doi.org:10.1128/mBio.02764-19
484 49 Buchanan, C. J. *et al.* Pathogen-sugar interactions revealed by universal saturation transfer
485 analysis. *Science* **377**, eabm3125 (2022). https://doi.org:10.1126/science.abm3125
486 50 Kistler, K. E. & Bedford, T. An atlas of continuous adaptive evolution in endemic human viruses.
487 *Cell Host Microbe* **31**, 1898-1909 e1893 (2023). https://doi.org:10.1016/j.chom.2023.09.012
488 51 Wells, H. L. *et al.* The coronavirus recombination pathway. *Cell Host Microbe* **31**, 874-889
489 (2023). https://doi.org:10.1016/j.chom.2023.05.003
490 52 Gut, M., Leutenegger, C. M., Huder, J. B., Pedersen, N. C. & Lutz, H. One-tube fluorogenic
491 reverse transcription-polymerase chain reaction for the quantitation of feline coronaviruses.
492 *J Virol Methods* **77**, 37-46 (1999). https://doi.org:10.1016/s0166-0934(98)00129-3
493 53 Sayers, E. W. *et al.* Database resources of the national center for biotechnology information.
494 *Nucleic Acids Res* **50**, D20-d26 (2022). https://doi.org:10.1093/nar/gkab1112
495 54 Quick, J. *et al.* Multiplex PCR method for MinION and Illumina sequencing of Zika and other
496 virus genomes directly from clinical samples. *Nature Protocols* **12**, 1261-1276 (2017).
497 https://doi.org:10.1038/nprot.2017.066
498 55 Vierstraete, A. R. & Braeckman, B. P. Amplicon_sorter: A tool for reference-free amplicon
499 sorting based on sequence similarity and for building consensus sequences. *Ecol Evol* **12**,
500 e8603 (2022). https://doi.org:10.1002/ece3.8603
501 56 Li, H. Minimap2: pairwise alignment for nucleotide sequences. *Bioinformatics* **34**, 3094-3100
502 (2018). https://doi.org:10.1093/bioinformatics/bty191

57 Altschul, S. F., Gish, W., Miller, W., Myers, E. W. & Lipman, D. J. Basic local alignment search tool. *J Mol Biol* **215**, 403-410 (1990). https://doi.org:10.1016/s0022-2836(05)80360-2

58 Robinson, J. T. *et al.* Integrative genomics viewer. *Nature Biotechnology* **29**, 24-26 (2011). https://doi.org:10.1038/nbt.1754

59 Amanda, W. *et al.* No part gets left behind: Tiled nanopore sequencing of whole ASFV genomes stitched together using Lilo. *bioRxiv*, 2021.2012.2001.470769 (2021). https://doi.org:10.1101/2021.12.01.470769

60 Katoh, K., Misawa, K., Kuma, K. i. & Miyata, T. MAFFT: a novel method for rapid multiple sequence alignment based on fast Fourier transform. *Nucleic Acids Research* **30**, 3059-3066 (2002). https://doi.org:10.1093/nar/gkf436

61 Kumar, S., Stecher, G. & Tamura, K. MEGA7: Molecular Evolutionary Genetics Analysis Version 7.0 for Bigger Datasets. *Mol Biol Evol* **33**, 1870-1874 (2016). https://doi.org:10.1093/molbev/msw054

62 Nguyen, L. T., Schmidt, H. A., von Haeseler, A. & Minh, B. Q. IQ-TREE: a fast and effective stochastic algorithm for estimating maximum-likelihood phylogenies. *Mol Biol Evol* **32**, 268-274 (2015). https://doi.org:10.1093/molbev/msu300

63 Rambaut, A., Lam, T. T., Max Carvalho, L. & Pybus, O. G. Exploring the temporal structure of heterochronous sequences using TempEst (formerly Path-O-Gen). *Virus Evolution* **2** (2016). https://doi.org:10.1093/ve/vew007

64 Letunic, I. & Bork, P. Interactive Tree Of Life (iTOL) v5: an online tool for phylogenetic tree display and annotation. *Nucleic Acids Research* **49**, W293-W296 (2021). https://doi.org:10.1093/nar/gkab301

65 Silva, G. G. Z. *et al.* Combining de novo and reference-guided assembly with scaffold_builder. *Source Code for Biology and Medicine* **8**, 23 (2013). https://doi.org:10.1186/1751-0473-8-23

66 Thompson, J. D., Higgins, D. G. & Gibson, T. J. CLUSTAL W: improving the sensitivity of progressive multiple sequence alignment through sequence weighting, position-specific gap penalties and weight matrix choice. *Nucleic Acids Res* **22**, 4673-4680 (1994). https://doi.org:10.1093/nar/22.22.4673

67 Waterhouse, A. *et al.* SWISS-MODEL: homology modelling of protein structures and complexes. *Nucleic Acids Res* **46**, W296-W303 (2018). https://doi.org:10.1093/nar/gky427

535 ## Methods

536 ### Enrolment of FIP cases in Cyprus

537 The electronic records of Vet Dia Gnosis Ltd in Limassol, Cyprus (at present, the only Veterinary
538 diagnostics lab on the island), were searched for any positive FCoV RT-PCR or IHC cases from
539 September 2021 up to June 2024. The cases to be enrolled needed to have compatible
540 clinicopathological findings for FIP as recently outlined by the European Advisory Board on Cat
541 Diseases Guidelines[25] as well having a positive FCoV IHC (on tissue biopsies with granulomatous
542 lesions) or a positive RT-PCR for FCoV in one of the following samples: peritoneal fluid, pleural
543 fluid, cerebrospinal fluid and granuloma fine needle aspiration biopsies or tissue biopsies. The
544 original samples were submitted to the Vet Dia Gnosis Ltd commercial laboratory (Limassol,
545 Cyprus) by local veterinarians and then submitted to LABOKLIN commercial laboratory (Bad
546 Kissingen, Germany). Ethical approval for this study was granted by the Pancyprian Vet
547 Association. According to the terms and conditions of the Vet Dia Gnosis, as well as the Cypriot
548 legislation [The Dogs LAW, N. 184 (I)/2002], no special permission from animal owners or the
549 animal welfare commission is needed for additional testing on residual sample material once
550 diagnostics are completed. According to the terms and conditions of the LABOKLIN laboratory, as
551 well as the RUF-55.2.2.2532-1-86-5 decision of the government of Lower Franconia, no special
552 permission from animal owners or the animal welfare commission is needed for additional
553 testing on residual sample material once diagnostics are completed. The study was also approved
554 by the Veterinary Ethical Review Committee, The Royal (Dick) School of Veterinary Studies
555 (R(D)SVS), The University of Edinburgh, UK (VERC Reference: 233.23).

556 ### Sample from cat imported to the UK

557 Two UK veterinary practices contacted the R(D)SVS with suspected cases of FIP in cats recently
558 imported from Cyprus. Peritoneal fluid samples were taken from the cats and sent to R(D)SVS for
559 further testing and for sequencing at The Roslin Institute with the consent of the cats' owners.
560 The veterinary practices and the cats' owners were kept informed at all stages.

561 ### Histopathology and immunohistochemistry

562 A sub-set of cases (n=4) from 17 non-effusive (dry) FIP cats diagnosed after January 2023 with
563 available tissue specimens were selected. Tissue specimens were carefully obtained and
564 immediately fixed in 10% buffered formalin. Following fixation, the tissues were processed by
565 embedding, 4μm sectioning, and subsequent staining with hematoxylin and eosin (H&E). The
566 inclusion criteria were defined based on comprehensive histopathological assessments.
567 Specifically, emphasis was placed on identifying the characteristic FIP-associated histological
568 hallmarks, which encompassed vasculitis, phlebitis, and periphlebitis. Consecutive tissue sections
569 were mounted onto charged slides. Following pre-treatment for 5 min at 110°C in 0.01M pH 6

570 citrate buffer, slides were incubated for 30 min at room temperature with primary mouse
571 monoclonal anti-feline coronavirus antibody at 1:400 (BioRad, MCA 2194). The EnVision anti-
572 mouse system was used for visualization according to the manufacturer's instructions (Agilent).

573 **RNA extraction and cDNA synthesis**

574 RNA from specimens from Cyprus underwent automated total nucleic acid extraction using the
575 MagNA Pure 96 DNA AND Viral NA Small Volume kit (Roche Diagnostics). RT-PCR for FCoV was
576 performed at Laboklin Bad Kissingen, Germany[52].

577 RNA samples from cats imported to the UK from Cyprus were extracted using the QIAamp viral
578 RNA extraction kit (Qiagen) according to the manufacturer's instructions.

579 cDNA synthesis on all RNA samples was carried out using LunaScript RT SuperMix Kit (NEB) with
580 16 µl template RNA in 20 µl reactions according to the manufacturer's instructions.

581 **Primer design and PCR amplification**

582 A set of primers for 1 kb /100 bp overlap tiled amplification were initially designed with available
583 FCoV genomes on NCBI[53] using primalscheme[54], and by manual redesign (Supplementary Table
584 S19). These were used to generate a composite representative FCoV-23 genome. Using this
585 genome a new, 800bp/80 bp overlap primer scheme was generated to sequence FCoV-23. The
586 primer sequences used here are found in (Supplementary Table S20). The PCRs for these
587 multiplexed amplifications used the same conditions described below, but with multiplexed
588 primers.

589 For a subset of samples, DNA was amplified using primers only targeting parts of spike, ORF1b,
590 and ORF3c/E/M. These primers may be found in (Supplementary Table S19, first four rows).

591 cDNA synthesis was performed using LunaScript reverse transcriptase Supermix (NEB) followed
592 by PCR amplification with Q5 (NEB). 1.25µl 10µM forward and reverse primers and 3µl cDNA in
593 a 25µl reaction. Amplification was performed with the following PCR conditions: initial
594 denaturation at 98°C for 30 seconds, 40 cycles of denaturation at 98°C for 10 seconds, annealing
595 and extension at 65°C for 4 minutes, followed by a final extension at 65°C for 5 minutes. Amplified
596 DNA was purified using AMPure XP beads (Beckman Coulter).

597 **Nanopore sequencing**

598 Amplicons were quantified using Qubit (Thermo Fisher) High Sensitivity assays and diluted to
599 150ng DNA per sample in 12µl nuclease-free water. Libraries were prepared using Oxford
600 Nanopore Technologies' (ONT) NBD112.96 ligation kit following the manufacturer's protocol for
601 amplicon sequencing with some modifications. Due to unavailability of NBD112.96 kit reagent
602 AMII H, following ligation of barcodes a second end-prep was carried out using the Ultra II End
603 Repair module (NEB). The rest of the protocol was carried out from the adapter ligation stage as

604 per manufacturer's protocol for LSK112 using the AMX-F adapter supplied in the early access
605 Q20+ version of kit 112. The library was loaded onto a MinION R10.4 flow cell and sequencing
606 was carried out on a GridION sequencing device.

607 In order to identify the virus present in one of the UK cases as quickly as possible, only the spike
608 amplicon was amplified and the sample sequenced using ONT RAD004 rapid sequencing kit on
609 an R9.4 flow cell following manufacturer's protocol. The other UK case was amplified at an earlier
610 time and was included in a sequencing run with the Cypriot samples, the data from that sample
611 was treated in the same way as the Cypriot samples and was the sample later found to have the
612 non-recombinant FCoVI spike.

613 **Bioinformatic analysis**

614 Basecalling and demultiplexing was carried out on the GridION sequencing device (ONT) using
615 Guppy (v2.24-r1122) on super accurate mode, specifying --require_barcodes_both_ends and
616 using appropriate super accurate basecalling models for each of the different sequencing
617 methods used. For the spike amplicons, following basecalling, amplicon_sorter[55] (v2023-06-19)
618 was used to identify consensus amplicons between 3kb and 5kb without using a reference. Spike
619 amplicons were identified from the output via alignment with minimap2[56] (v2.22) to the spike
620 from the first sample we sequenced (1-G7_Gi_6739) for which a consensus was made using the
621 same process, with the correct amplicon identified via BLAST[57]. The identified amplicons were
622 polished with medaka (v1.8.0, ONT). For the UK case which was sequenced with the rapid kit,
623 because the reads were fragmented by the library prep process, reads were used to polish the 1-
624 G7_Gi_6739 sequence using medaka. The reads were aligned to the polished sequence with
625 minimap2 and visualized with IGV[58] (v2.11.1) to visually confirm the reads supported the
626 consensus sequence and that it had not been biased by the reference used. The amplicons in
627 POL1ab and Orf3c/E/M were assembled and polished using LILO[59]. Multisequence alignments
628 were carried out for each of the regions using mafft[60] (v7.49) against all complete genomes of
629 CCoV and FCoV genomes available on NCBI using the --adjustdirection flag. Alignments were
630 visualized in Mega7[61]. All downloaded genomes were trimmed down to each of the target regions
631 amplified from our samples. Maximum likelihood trees were constructed using IQ-TREE[62]
632 (v2.0.5). TempEst[63] (v1.5.3) was used to determine the best fitting root for the trees, and
633 visualizations and annotations of the trees were done using iTOL[64] (v6.8.1).

634 To assemble a representative genome for the population, the combined reads of several samples
635 for which we had sequencing data were run through LILO. The polished amplicons were mapped
636 to a single fasta file containing an FCoVI (MT239440.1) and a CCoVII (KP981644.1) using
637 minimap2 and visualized with IGV, with only the amplicons from the spike region aligning to
638 CCoVII. Representative amplicons covering the entire genome were selected and scaffolded using

639 scaffold_builder[65] with MT239440.1 as a reference. The raw reads were trimmed by 50bp to
640 remove adapters and barcodes and they were used to polish this scaffold using medaka. Mafft
641 was used to align this genome to representative genomes from *Alphacoronavirus 1* with Canine
642 Respiratory Coronavirus as an outgroup, and Mega7 was used to create a neighbor join tree which
643 was visualized and annotated with iTOL.

644 Having assembled a representative genome, primers were redesigned to include ambiguous
645 bases that supported the sequence in the representative genome, and these are the primers that
646 were used to amplify 800bp tiled amplicons for individual Cypriot samples. The Cypriot samples
647 were assembled using LILO, with the representative genome as the reference. Assembled
648 genomes had their reads aligned back to them using minimap2 and were visualised with IGV.
649 Each genome was visually inspected for errors and corrections made, primarily where primer
650 sequences had been incorrectly incorporated. Where there were gaps in these genomes, and
651 there were reads that spanned the gap but did not reach the depth threshold for LILO, reads were
652 extracted and amplicon_sorter was used to attempt to create a consensus for the missing
653 amplicon. These amplicons were carefully visually inspected for errors before being incorporated
654 into the assembly to close gaps using scaffold_builder. Multisequence alignments between the
655 population level representative genome. a sample without a spike domain 0 deletion (2-
656 C11_Re_10276) and a sample with a domaion 0 deletion (2-F12_Bl_11350) against MT239440.1,
657 LC742526.1 and KP981644.1 was carried out using ClustalW[66] in Mega7, and recombination
658 analyses carried out using RDP5[37] (v.5.45) on default settings.

659 **Structure prediction of spike deletion variants**

660 SWISS-MODEL structure prediction and analysis (https://swissmodel.expasy.org/, accessed
661 October 2023)[67] were used to model the partial, high confidence N-terminal sequence of a
662 full-length spike (1008aa) and a deletion spike (797aa). To model the G8 Cypriot full-length spike,
663 we used the alphacoronavirus 1 experimentally resolved CCoV-HuPn-2018[40] structure as a
664 template. Modelling against the 7usa.1.a, swung out confirmation, yielded GMQE 0.60 and Global
665 QMEAND of 0.68±0.05 with a sequence identity of 88.97% and against 7us6.1.A, proximal
666 confirmation, yielded GMQE of 0.62 and Global QMEAND of 0.58±0.05 with a sequence identity of
667 81.03%. Modelling of C10 spike, C-terminal deletion, against 7usa.1.A, swung out confirmation,
668 yielded GMQE 0.74 and Global QMEAND of 0.69±0.05 with a sequence identity of 88.66% and
669 against 7us6.1.A, proximal confirmation of HuPN, yielded GMQE of 0.76 and Global QMEAND of
670 0.70±0.05 with a sequence identity of 88.42%.

671 The receptor binding domain was modelled using the 7u0I.1B structure, again CCoV-HuPn-
672 2018[40] complexed with canine APN as a template. GMQE was 0.89 and Global QMEAND 0.85±0.07
673 with a sequence identity of 92.41%. PDB files are available in the supplementary materials.

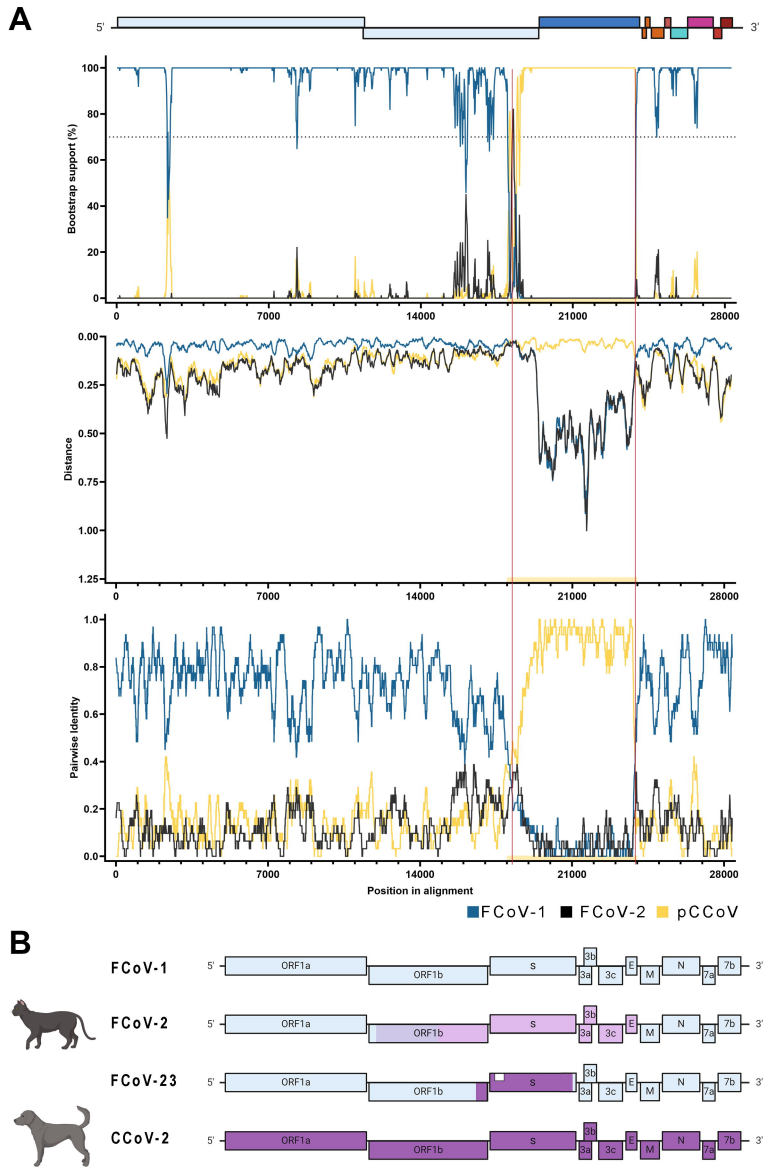
A
5'
3'
Bootstrap support (%)
100
80
60
40
20
0
0
7000
14000
21000
28000
Distance
0.00
0.25
0.50
0.75
1.00
1.25
Pairwise Identity
1.0
0.8
0.6
0.4
0.2
0.0
Position in alignment
FCoV-1
FCoV-2
pCCoV
B
FCoV-1
FCoV-2
FCoV-23
CCoV-2
ORF1a
ORF1b
S
3b
3a
3c
E
M
N
7a
7b

A

## FCoV-23 Spike

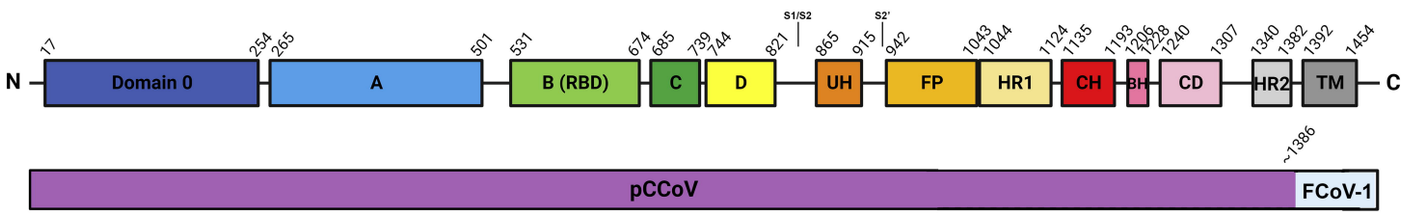


### Domain 0 deletion

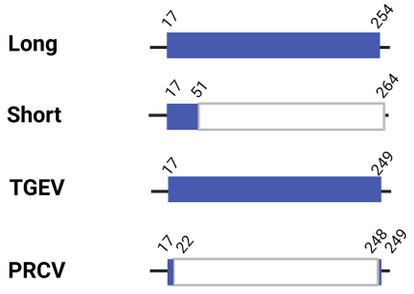


### Significant amino acid changes

| Domain | A | | | | B (RBD) | | | | | | | | C | | D | UH | FP | HR1 | CH | BH | CD | HR2 |
|---|---|---|---|---|---|---|---|---|---|---|---|---|---|---|---|---|---|---|---|---|---|---|
| Position | 291 | 384 | 403 | 458/59 | 531/32 | 535 | 546 | 556 | 595 | 605 | 636 | | 699 | 702 | 754 | | | 1096 | | | 1248 | |
| **FECV-2** AB097624 | S | S | R | GA | FA | A | R | T | N | Y | N | | R | V | A | no unusual aa changes | no unusual aa changes | Q | no unusual aa changes | no unusual aa changes | R | no unusual aa changes |
| **FECV-2** AB781788 | S | S | R | GA | LT | A | R | S | I | Y | S | | R | V | A | | | Q | | | R | |
| **FECV-2** AB781789 | S | S | R | GA | FA | A | R | T | N | G | N | | R | V | A | | | Q | | | R | |
| **FECV-2** JN634064 | S | S | R | GD | FA | A | R | T | I | D | S | | R | V | A | | | K | | | R | |
| **FIPV-2** JQ408981 | S | S | R | GA | FT | A | L | T | I | E | S | | R | V | A | | | Q | | | R | |
| **FIPV-2** MK987175 | S | R | R | GV | FT | A | L | T | I | E | S | | R | V | A | | | Q | | | R | |
| **FIPV-2** GQ152141 | S | S | R | GA | FA | A | R | T | N | Y | N | | R | V | A | | | Q | | | R | |
| **FIPV-2** X06170 | S | S | R | GV | FT | A | L | T | I | E | S | | R | V | A | | | Q | | | R | |
| **FCoV-23** consensus | D | R | K | ST | YS | S | L | A | V | H | H | | K | I | T | | | K | | | H | |
| **FCoV-23** C10_short | D | R | K | ST | YS | S | L | A | V | H | H | | K | I | T | | | K | | | H | |
| **FCoV-25** G8_long | D | R | K | ST | YS | S | L | A | V | H | H | | K | I | T | | | K | | | H | |
| **pCCoV** CB/05 | G | S | R | GT | YS | S | R | A | V | H | N | | R | V | A | | | K | | | R | |

B

## Variations in spike deletion in 57 cats

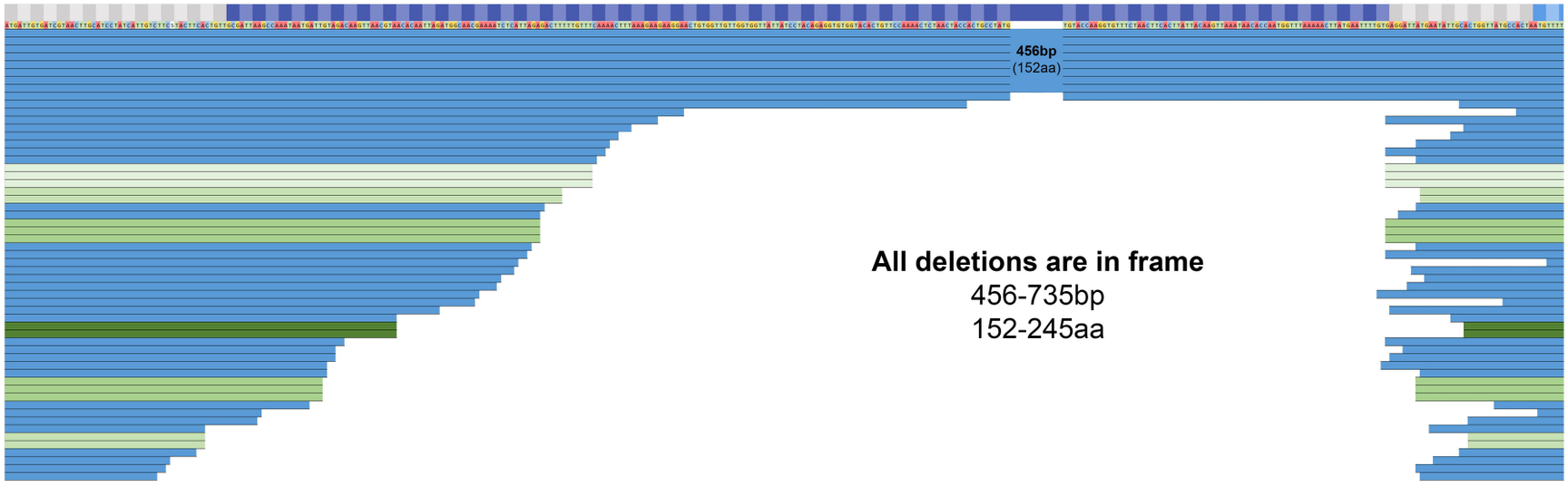


C

## G8 - long spike

Structure prediction

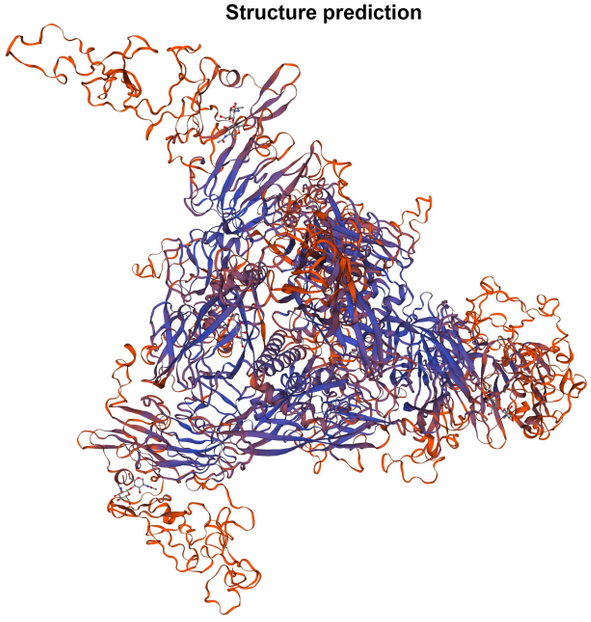

## C10 - short spike

Structure prediction

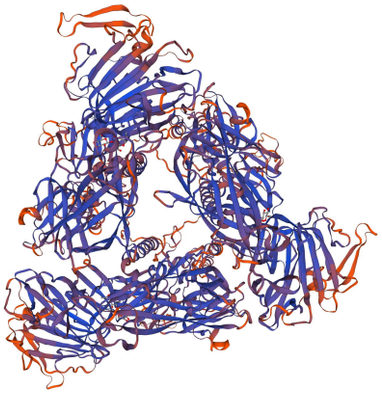

D

## RBD

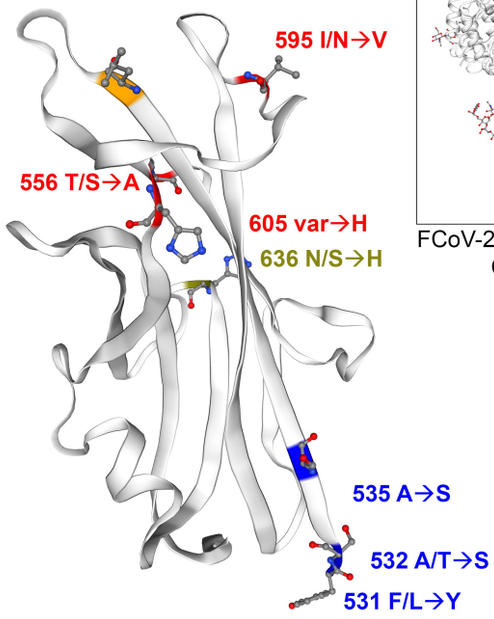


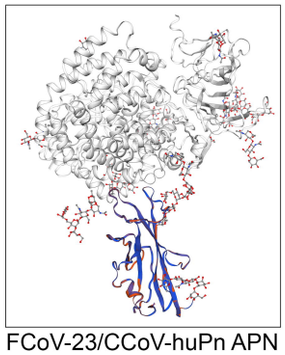

FCoV-23/CCoV-huPn APN Comparison

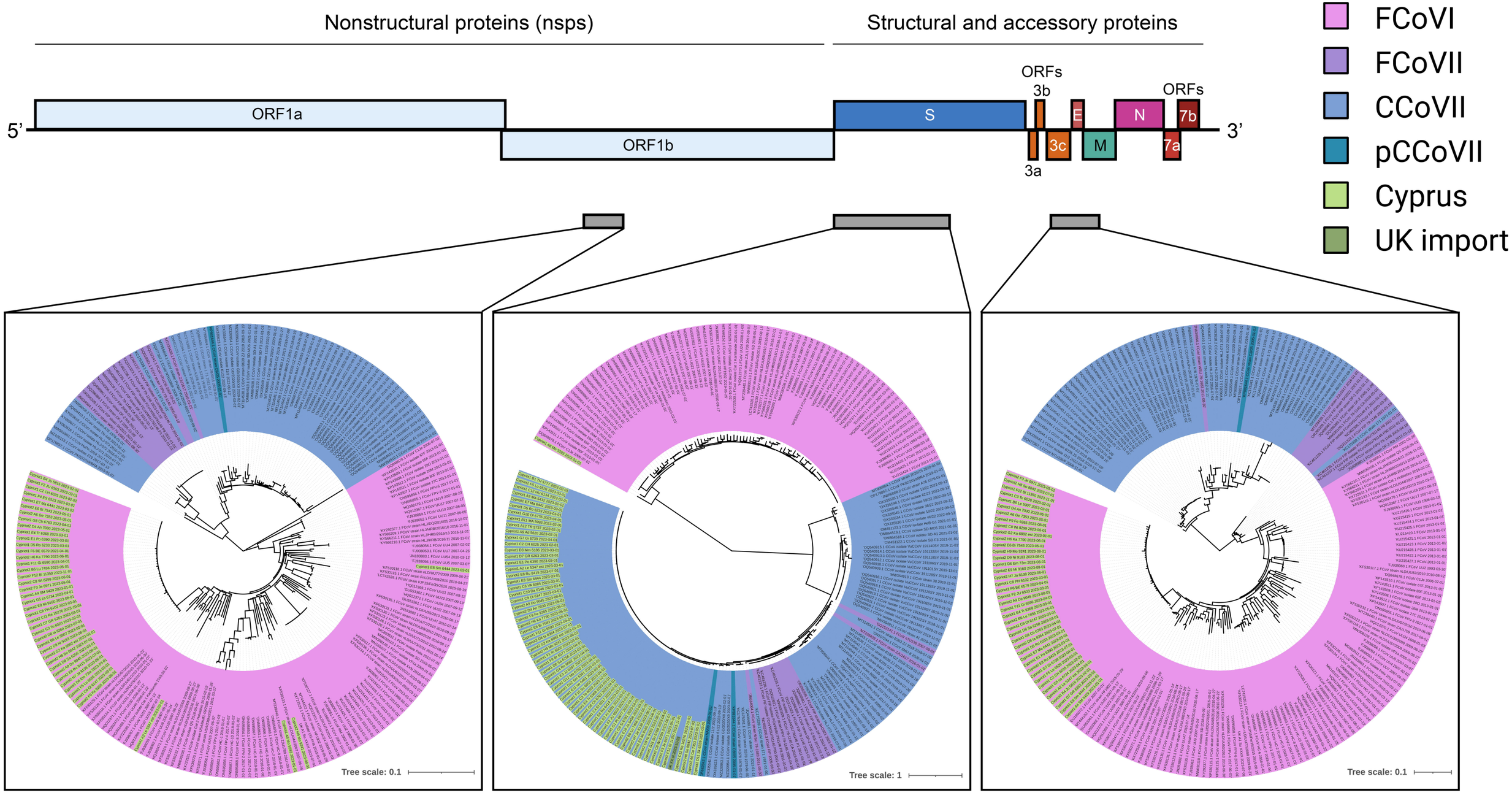
Nonstructural proteins (nsps)
Structural and accessory proteins
5'
ORF1a
ORF1b
S
ORFs
3b
3a
3c
E
M
N
ORFs
7b
7a
3'
FCoVI
FCoVII
CCoVII
pCCoVII
Cyprus
UK import
Tree scale: 0.1
Tree scale: 1
Tree scale: 0.1

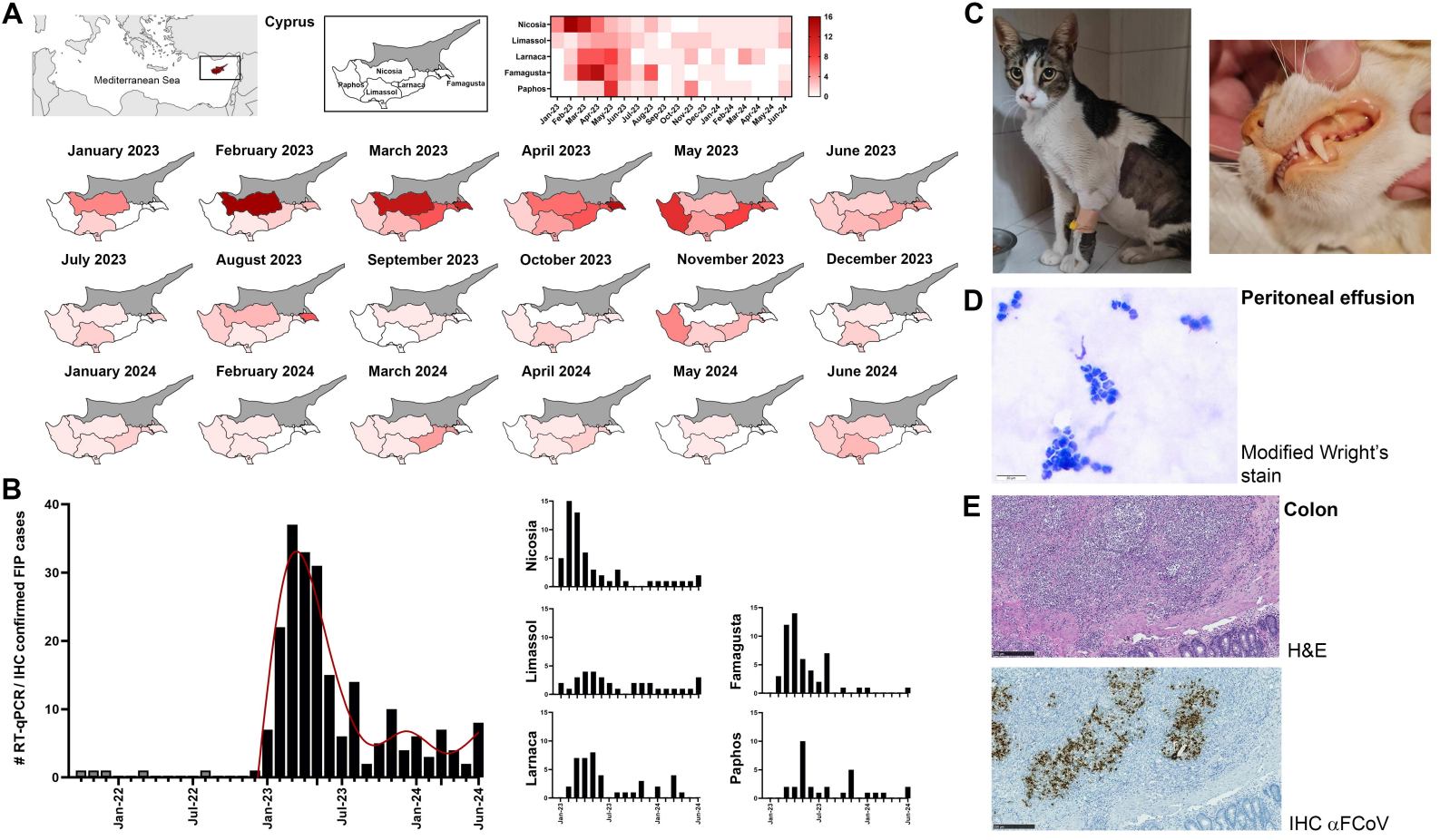
A
Mediterranean Sea
Cyprus
Nicosia
Paphos
Larnaca
Limassol
Famagusta
Nicosia
Limassol
Larnaca
Famagusta
Paphos
Jan-23
Feb-23
Mar-23
Apr-23
May-23
Jun-23
Jul-23
Aug-23
Sep-23
Oct-23
Nov-23
Dec-23
Jan-24
Feb-24
Mar-24
Apr-24
May-24
Jun-24
16
12
8
4
0
January 2023
February 2023
March 2023
April 2023
May 2023
June 2023
July 2023
August 2023
September 2023
October 2023
November 2023
December 2023
January 2024
February 2024
March 2024
April 2024
May 2024
June 2024
B
# RT-qPCR / IHC confirmed FIP cases
40
30
20
10
0
Jan-22
Jul-22
Jan-23
Jul-23
Jan-24
Jun-24
Nicosia
Limassol
Larnaca
Famagusta
Paphos
15
10
5
0
Jan-23
Jul-23
Jan-24
Jun-24
C
D
Peritoneal effusion
Modified Wright's stain
E
Colon
H&E
IHC αFCoV